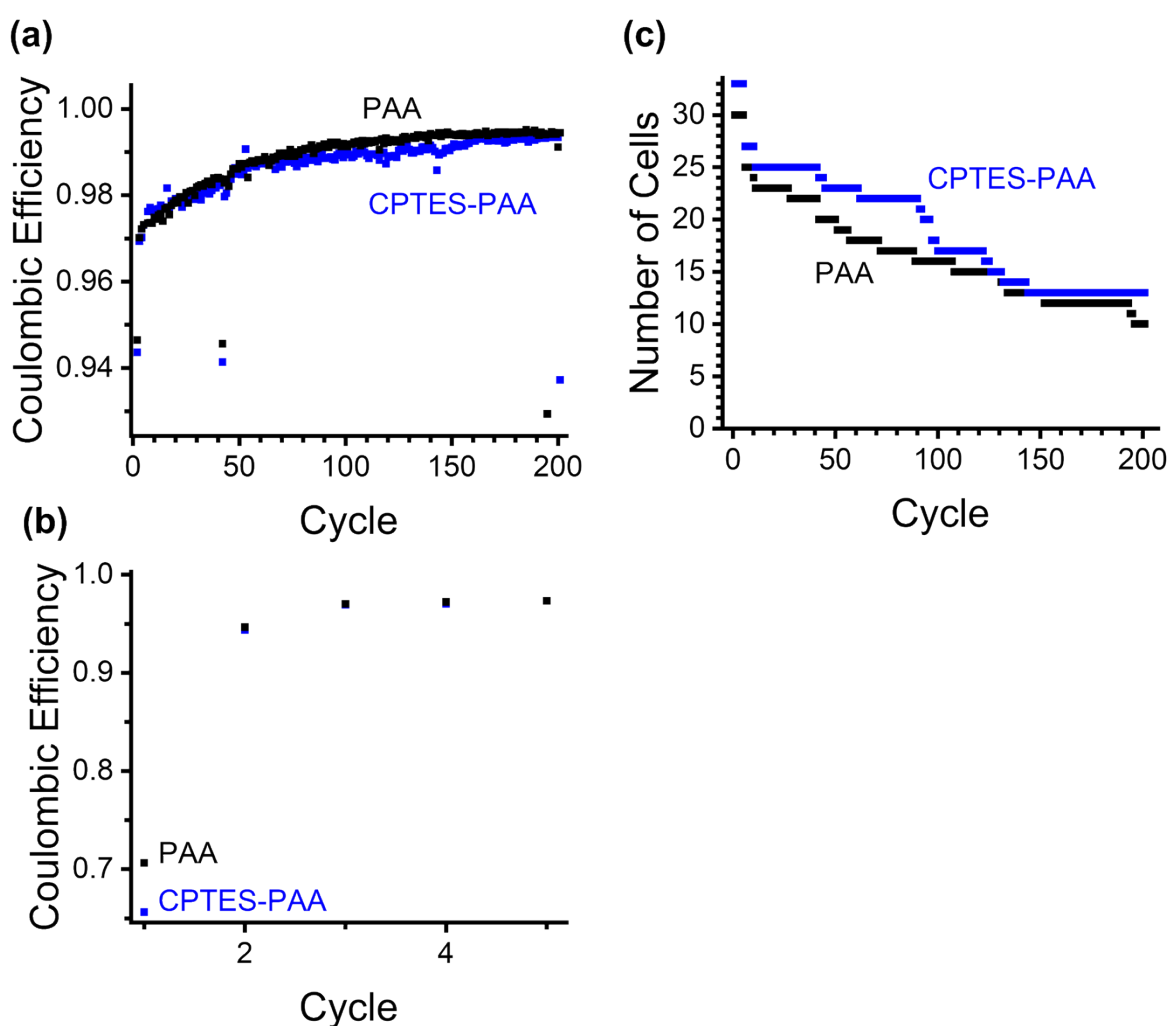# Supplemental Information for Selective Kinetic Control of Interfacial Charge Transfer Reactions in Si-composite Anodes for Li-ion Batteries

Fig. S1. Magnification of coulombic efficiencies for PAA (black) and PAA-CPTES (blue) 50nm SiNP cells for cycles 2-201 (a) and cycles 1-5 (b). Number of cells of each type that were used for statistical values reported as a function of the cycle number (c). Due to limitations on instrument time, not all cycles were cycled the same number of times.

Fig. S1a and b above are the coulombic efficiency data shown in the main paper, scaled to show in more detail. Fig. S1c is a count of the number of each type of cell that were cycled to a given number of cycles, expanding on the information provided in the main paper.
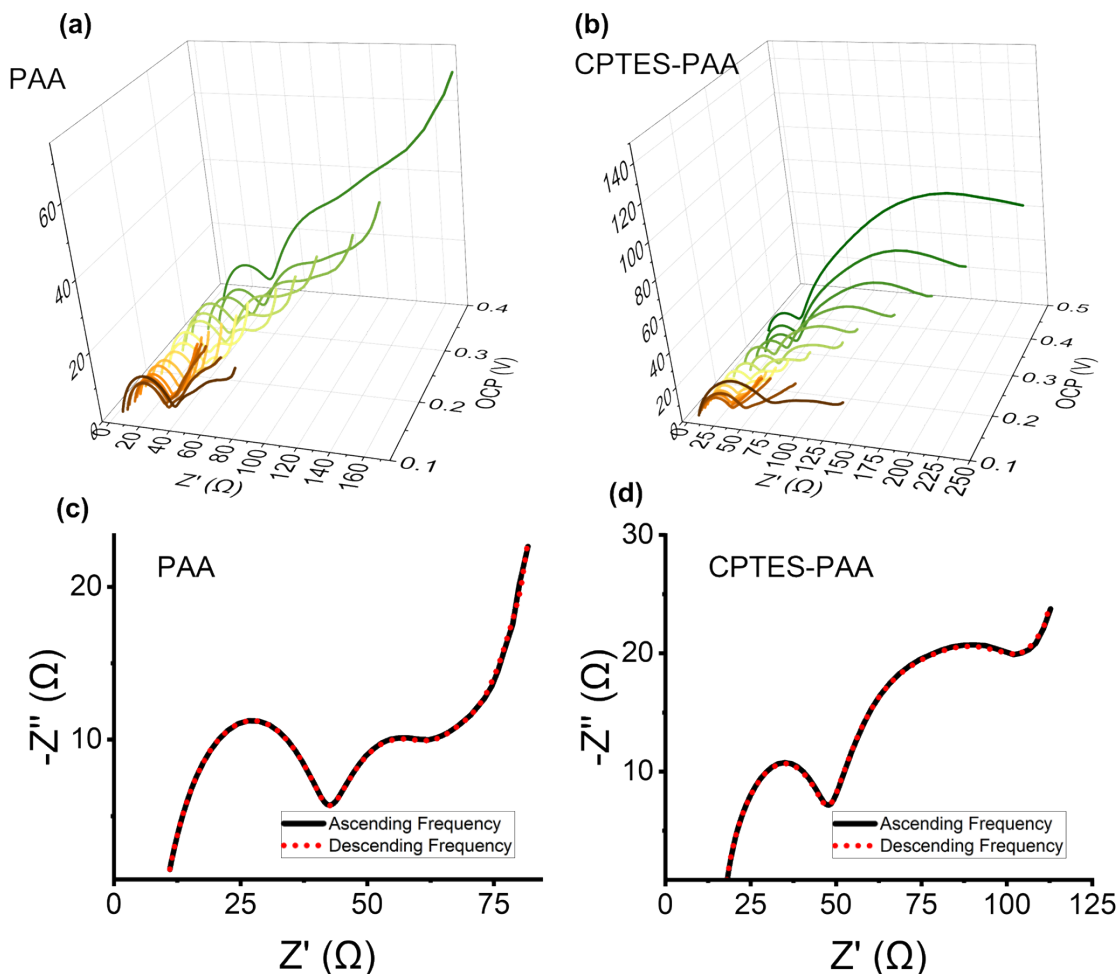
Fig. S2. Nyquist plots over a range of voltages/states of charge for (a) PAA and (b) PAA-CPTES cells. Ascending and descending frequency order Nyquist plots for the (c) PAA and (d) PAA-CPTES cells and states of charge fitted and analyzed in this work.

Fig. S2 shows EIS Nyquist plots as a function of potential for 7 cycled PAA (a) and CPTES-PAA (b) cells. Fig. S2c and d show the ascending and descending frequency order data for the data displayed in the main text. The difference between the electrode formulations in the Z' value at the highest frequency point (or the difference in the solution resistance) is likely a function of the slight variability in the electrolyte wetting, electrolyte content, and general cell-to-cell fabrication variability. Such natural variability is accounted for in the fitting and, therefore, does not affect our analysis of the CT or SEI impedance parameters.

Calculations of SEI capacitance

Calculation of capacitance from constant phase elements parameters has been performed in various ways in literature. The following equations were used to evaluate the effective SEI capacitance (C) based on the fitted equivalent circuit parameters (method one is reported in the main text):

Method 1 (reported in text):[1]
$$C = \frac{(QR)^{1/n}}{R} \sin\left(\frac{n\pi}{2}\right)$$

Method 2:[1]
$$C = Q(\omega_{max}^n)^{n-1}$$

Method 3:[2]
$$C = \frac{(QR)^{1/n}}{R}$$

Method 4:[3]
$$C = \frac{Q(\omega_{max}^n)^{n-1}}{\sin\left(\frac{n\pi}{2}\right)}$$

Method 5:[4]
$$C = \left(\frac{Q}{(R_\Omega^{-1} + R^{-1})^{1-n}}\right)^{1/n}$$

For all methods, R is the resistance in parallel, Q is the CPE magnitude parameter, and n is the CPE exponent parameter. ω_{max} is the angular frequency at which the negative of the imaginary part of the resistance for the fitted R-CPE circuit reaches it's maximum. R_Ω is the fitted solution resistance. Table S1 shows the frequencies used in the methods that require it, the SEI capacitance (C_{SEI}) values for the PAA and CPTES-PAA cells calculated by each method (using the R, Q, and n values for the SEI impedance element), and the ratio between them for each method, as well as the average of the capacitance and ratios across the methods.

	PAA	PAA-CPTES	Capacitance ratio (PAA-CPTES:PAA)
ω_{max} from R-CPE fit (angular Hz)	11512	7214	
C_{SEI} *(Method 1, µF)*	2.291	4.800	2.095
C_{SEI} (Method 2, µF)	2.529	5.068	2.004
C_{SEI} (Method 3, µF)	2.472	5.220	2.112
C_{SEI} (Method 4, µF)	2.344	4.660	1.988
C_{SEI} (Method 5, µF)	1.567	3.710	2.368
Average C_{SEI} (µF)	**2.282**	**4.879**	**2.150**
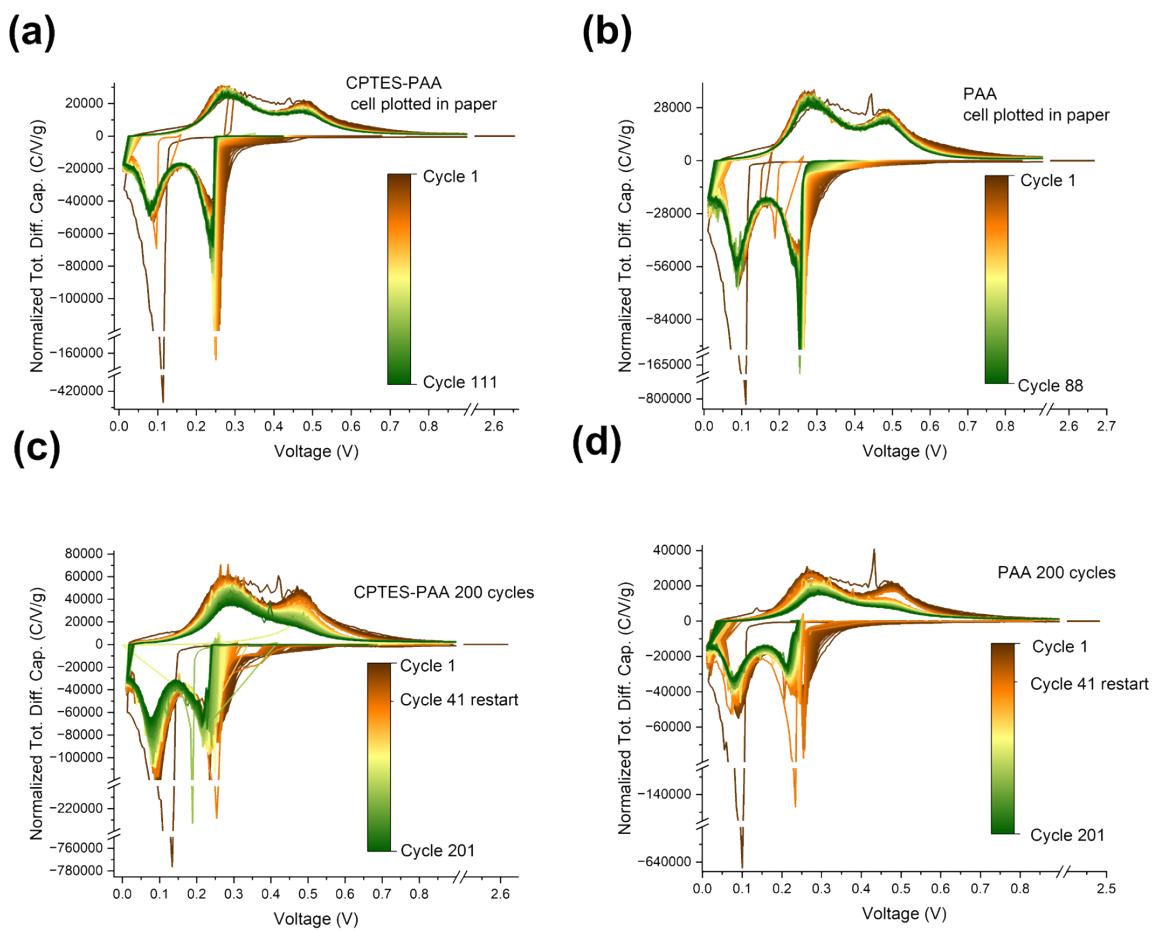
Fig. S3. Full differential capacity Data for PAA-CPTES (a,c) and PAA (b,d) cell differential capacity shown in paper (a,b), other representative cells cycled 200 times (c,d)

Fig. S3 provides full differential capacity traces for cells fabricated on the same date (a and b, c and d, are pairs of CPTES-PAA cells and PAA cells fabricated at the same time). These are provided here in order to reduce clutter in the figures in the main text.
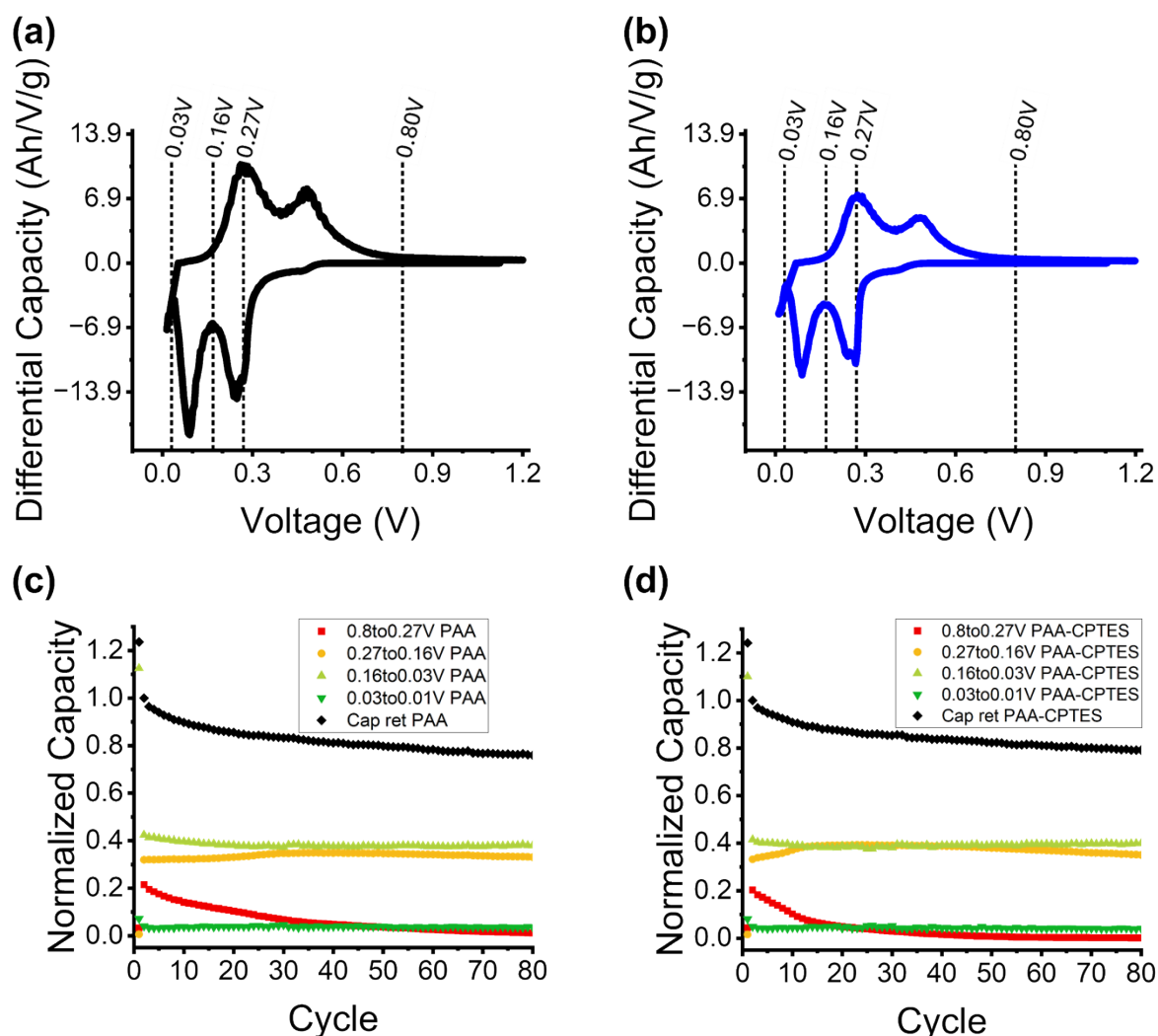
Fig. S4. Voltage windows during lithiation 0.8-0.27V (R1), 0.27-0.16V (R2), 0.16-0.03V (R3), and 0.03-0.01V (R4) over 80 cycles used for analysis for PAA (a) and CPTES-PAA (b). Capacity in those voltage windows for PAA (c) and CPTES-PAA (d) cells. The capacity values in each window are normalized to the total lithiation capacity of the 2nd cycle. Black traces are the capacity retention (normalized to the 2nd cycle).

Fig. S4 shows an analysis analogous to that done by Lucht et al. in 2015, wherein the differential capacity trace is used as a guide to split the charging data into voltage regions. These regions are then tracked across cycles to indicates what potential range changes in capacity are derived from.[5] As the voltage ranges used in that analysis work well for our differential capacity data as well, we use the same ones (with the exception of the lowest potential range – the lowest potential our cells were lithiated to was 0.01V vs. Li/Li$^+$, so that is the lower bound).

Lucht et al. observed a sequential fading mechanism, where R1 was responsible for the majority of capacity decay over early cycles, and then, once the capacity in R1 decayed to zero, R2 took over as the primary contributor. We observe qualitatively different behavior:

- No plateau in R1 in early cycles,
- Much slower decay of R1 (especially for PAA cells),
- An increase in R2 as R1 decreases

These differences inform our interpretation of the pre-alloying region R1 in our system as containing not just reversible alloying reactions, but also other irreversible reactions.
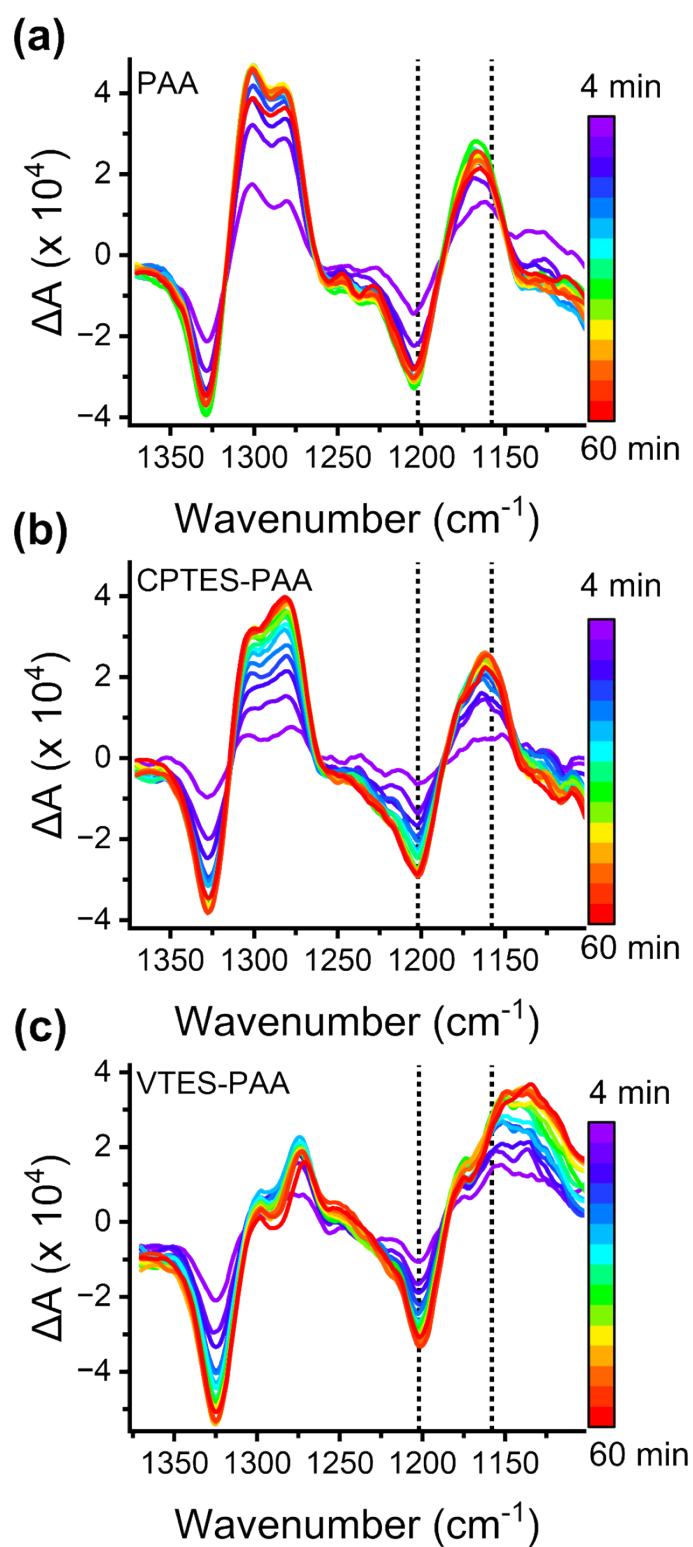
Fig. S6. ΔA spectra in the carbonate solvent signature window for PAA (a), CPTES-PAA (b), and VTES-PAA (c) binder films (no active material or conductive carbon present). Spectra taken during -1V vs. OCP hold step of ~ 1 hour.

Fig. S6 shows a wider spectral range for the in situ spectroelectrochemical vibrational spectra

than was analyzed in the main paper, as well as the spectra for modified binders. This shows the difference in the lithium coordinated ethylene carbonate region (around 1158 cm^{-1}) between modified and unmodified binders. These spectra also show the range where signals for the other organic carbonates in solution appear.
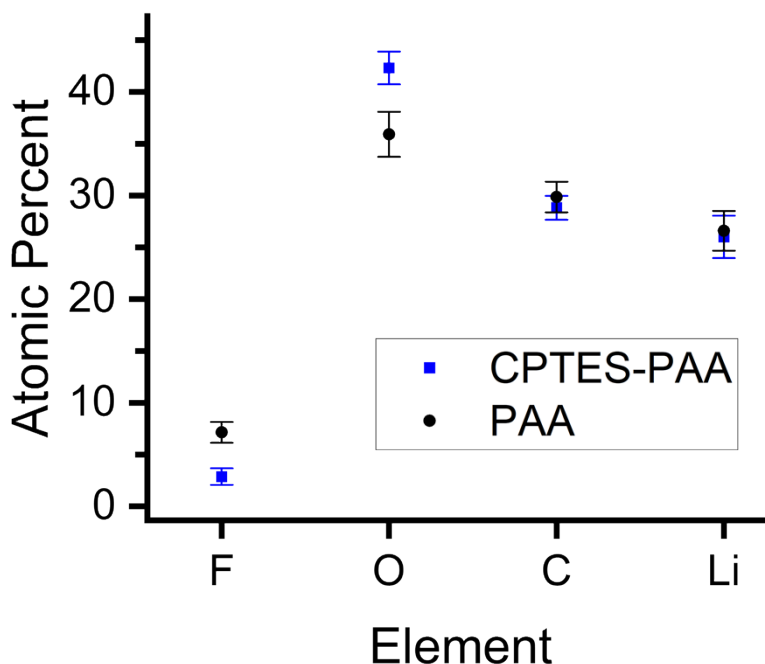
Fig. S7. Elemental composition averages for the 7 cycle SEI from PAA (black) and CPTES-PAA (blue) half cells from XPS analysis. Error bars indicate ± 1 standard deviation.

Fig. S7 shows the difference in fluorine and oxygen content in the SEI between CPTES-PAA cells and PAA cells, as well as the similarity in carbon and lithium. CPTES-PAA cells have a lower F content, but a higher O content than PAA cells, while retaining the same amount of Li. This indicates a higher degree of lithium in carbonate salts, rather than fluoride, and supports the idea that the modified binders preferentially exclude FEC from being reduced.
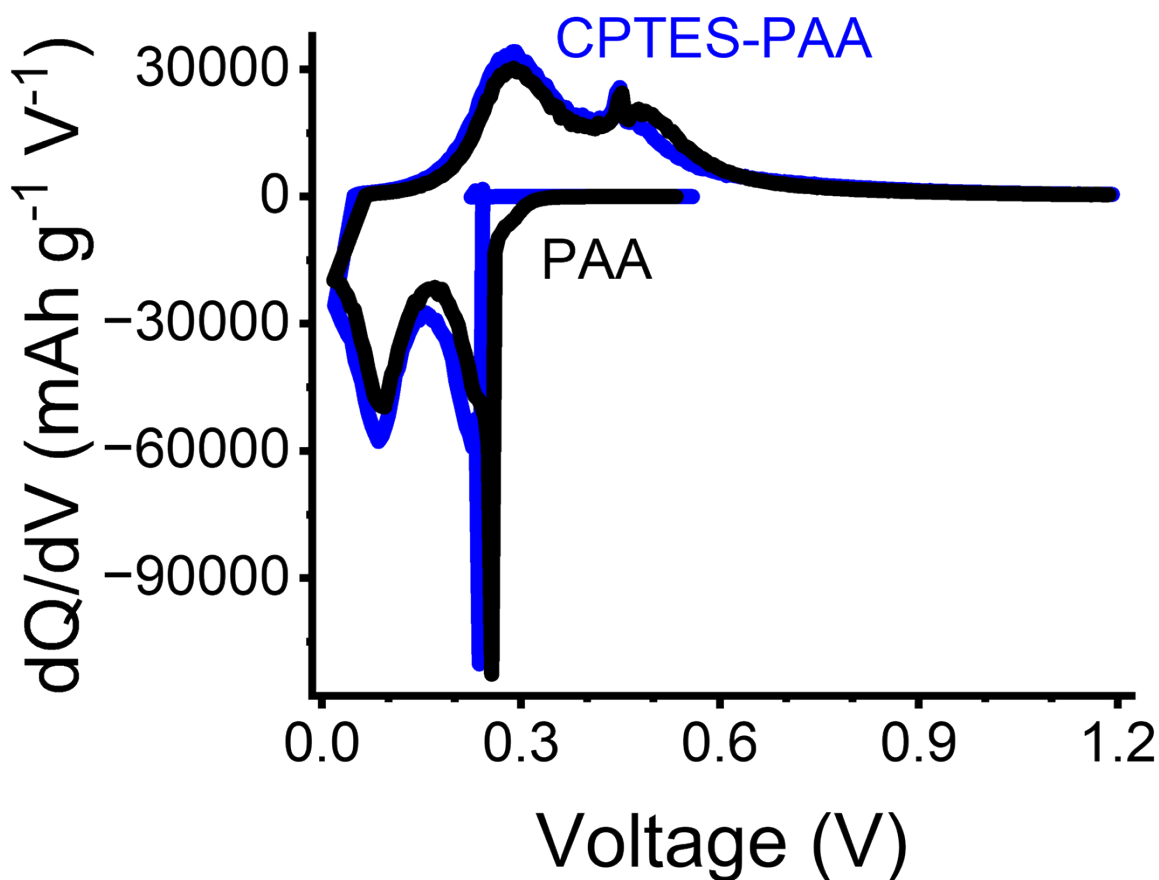
Fig. S8. Cycle 7 differential capacity traces for PAA (black) and CPTES-PAA (blue) cells made with FEC-free electrolyte (1M LiPF$_6$ in 1:1 EC:DMC).

Fig. S8 shows the dQ/dV traces of 50nm SiNP, FEC-free electrolyte fabricated half cells for CPTES-PAA and PAA electrodes. This shows that, despite the difference in FEC transport and reduction as indicated by the in situ FTIR binder measurements and XPS measurements of the SEI, the difference in overpotential in the pre-alloying voltage range seems not to be driven by this difference. Cells made without FEC show the same difference in overpotential (cycle 7 shown).
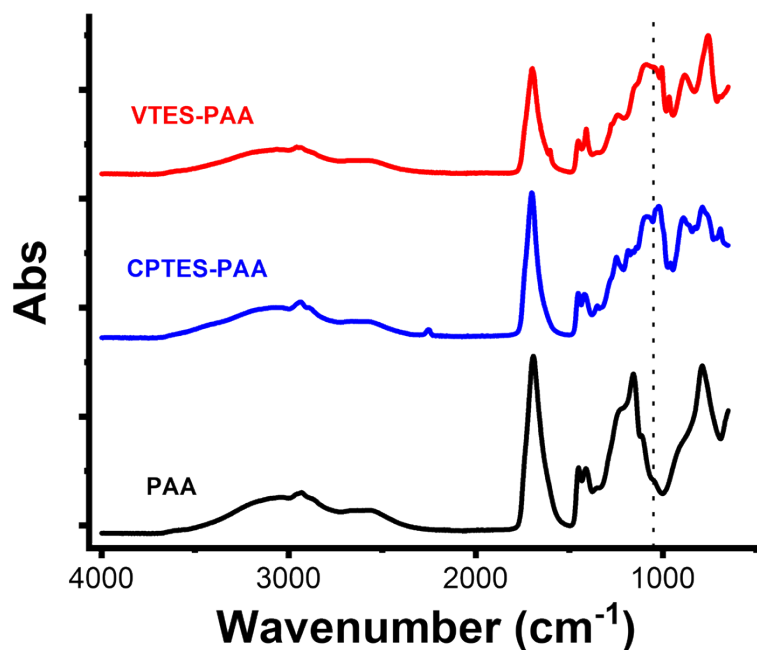
Fig. S9. FTIR spectra of PAA (black), CPTES-PAA (blue), and VTES-PAA (red) binder films.

Fig. S9 shows the full spectra for unmodified and modified binder films, showing the diagnostic peaks indicating successful modification (described in the main text). Note also the silane signals in the 1050 cm^{-1} region where the polyether signal from PAA is expected to be.[6]

References

1. B.-Y. Chang, *J. Electrochem. Sci. Technol.*, 2020, **11**, 318-321.
2. C. Liu, S. Busse, J. Liu and R. Godin, *ACS Appl. Mater. Interfaces.*, 2023, **15**, 46902-46915.
3. E. P. M. van Westing, G. M. Ferrari and J. H. W. de Wit, *Corros. Sci.*, 1993, **34**, 1511-1530.
4. G. J. Brug, A. L. G. van den Eeden, M. Sluyters-Rehbach and J. H. Sluyters, *J. Electroanal. Chem.*, 1984, **176**, 275-295.
5. T. Yoon, C. C. Nguyen, D. M. Seo and B. L. Lucht, *J. Electrochem. Soc.*, 2015, **162**, A2325-A2330.

6.   T. R. Martin, R. T. Pekarek, J. E. Coyle, M. C. Schulze and N. R. Neale, *J. Mater. Chem. A*, 2021, **9**, 21929-21938.